Spreading continents kick-started plate tectonics

Patrice F. Rey, Nicolas Coltice, Nicolas Flament

Spreading Continents Kick-Started Plate Tectonics

Patrice F. Rey[1], Nicolas Coltice[2] & Nicolas Flament[1]

[1]Earthbyte Research Group – School of Geosciences, The University of Sydney – Sydney NSW 2006, Australia.

[2]CNRS-UMR 5276, Laboratoire de géologie de Lyon, École Normale Supérieure et Université Claude Bernard, et Institut Universitaire de France; 69622 Villeurbanne cedex, France.

Plate tectonics characterises the present-day geodynamics of the Earth. Stresses acting on cold, thick and negatively buoyant oceanic lithosphere are key to the initiation of subduction and the operation of plate tectonics[1,2]. In the Archaean, because the Earth interior was hotter, oceanic crust may have been thicker, making oceanic lithosphere possibly more buoyant than at present[3]. Whether subduction and plate tectonics occurred on the early Earth is ambiguous both in the geological record and in geodynamic models[4]. Here we show that because they were thick and buoyant[5], early continents produced intra-lithospheric gravitational stresses large enough to drive their gravitational spreading, to initiate subduction at their margins, and to trigger subduction episodes. Our model predicts the co-occurrence of deep to progressively shallow mafic volcanics and arc magmatism within continents in a self-consistent geodynamic framework, explaining the enigmatic multimodal volcanism and tectonic record of Archaean cratons[6]. Moreover, our model predicts a progressive petrological stratification and tectonic structuration of the sub-continental lithospheric mantle, two predictions that are respectively consistent with xenolith[5] and seismic studies, and consistent with the existence of a mid-lithospheric seismic discontinuity[7]. The slow gravitational collapse of early continents could have kick-started transient plate tectonic episodes until, as the Earth interior cooled and oceanic lithosphere became heavier, plate tectonics became self-sustaining.

Present-day plate tectonics is primarily driven by the negative buoyancy of cold subducting plates. Petrological and geochemical proxies of subduction preserved in early continents point to subduction-like processes already operating before 3 billion years (Gyr) ago[8,9] and perhaps as early as 4.1 Gyr ago[10]. However, they are not unequivocal, and geodynamic modelling suggests that the thicker basaltic crust produced by partial melting of a hotter Archaean or Hadean mantle would have

increased lithospheric buoyancy and inhibited subduction[3,4]. Therefore, mantle convection under a stagnant lid with extensive volcanism could have preceded the onset of subduction[11]. In this scenario, it is classically assumed that the transition from stagnant-lid regime to mobile-lid regime and the onset of plate tectonics require that convective stresses overcame the strength of the stagnant lid[12] at some stage in the Archaean.

On modern Earth, gravitational stresses due to continental buoyancy can contribute to subduction initiation[2,13]. The role of continental gravitational stresses as a driver of Archaean lithospheric deformation has been emphasized[14,15], however their potential to initiate subduction has been overlooked. Studies of xenolith in Archaean cratons show that the early continental crust was underlain by a thick (~200 km), moderately- to strongly-depleted and therefore buoyant lithospheric mantle[5]. A common model for the formation of early continental lithosphere invokes partial melting in mantle plumes, leading to magnesium-rich mantle residues (e.g. refractory harzburgites and dunites) under thick basaltic plateaux[5,16,17]. Partial melting of these thick basaltic crusts, at depth >˜40 km, further differentiates the crust into tonalite-trondjemite-granodiorite (TTG) and restitic material[16,18].

First order calculations show that the horizontal gravitational force acting between a continent 200 km thick and adjacent oceanic lithosphere is of the order of 10^{13} N m^{-1} (see Extended Data Fig. 1), comparable to that of present-day tectonic forces driving orogenesis[1]. To explore the tectonic impact of a thick and buoyant continent surrounded by a stagnant lithospheric lid, we produced a series of two-dimensional thermo-mechanical numerical models of the top 700 km of the Earth, using temperature-dependent densities and visco-plastic rheologies depending on temperature, melt fraction and depletion, stress and strain rate (see Methods). The initial temperature field is the horizontally-averaged temperature profile of a stagnant-lid convection calculation for a mantle ~200 K hotter than at present (Fig. $1a_0$ and Extended Data Fig. 2). The absence of lateral temperature gradients ensures that no convective stresses act on the lid, allowing us to isolate the dynamic effect of the continent. A 225-km-thick, buoyant and stiff continent (170-km-thick strongly depleted mantle root overlain by 40-km-thick felsic crust; see Fig. $1b_1$) is inserted within the lid, on the left side of the domain to exploit the symmetry of the problem (Fig. $1a_0$). A 15-km-thick mafic crust covers the whole system

(Fig. 1a$_0$), accounting for the common occurrence of thick greenstone covers on continents, as well as thick basaltic crust on the oceanic lid[3].

Our numerical solutions show that the presence of a buoyant continent imparts a horizontal force large enough to induce a long period (~50 to 150 million years - Myr) of slow collapse of the whole continental lithosphere (Fig. 1 and Extended Data Fig. 3), in agreement with the dynamics of spreading for gravity currents[19]. Hence, a continent of larger volume leads to larger gravitational power and faster collapse. Because of lateral spreading of the continent, the adjacent lithospheric lid is slowly pushed under its margin (Fig. 1a$_1$, and Extended Data Fig. 3 a$_1$). For gravitational stress lower that the yield stress of the oceanic lid, thickening of the margin of the lid is slow and viscous drips (i.e. Rayleigh-Taylor instabilities) detach from its base (Extended Data Fig. 3 a$_{0\text{-}1}$). These instabilities, typical for stagnant-lid convection[20], mitigate the thermal thickening of the lid.

When gravitational stresses overcome the yield stress of the lithospheric lid, subduction is initiated (Figs. 1a$_{1\text{-}2}$). Depending on the half-width of the continent and its density contrast with the adjacent oceanic lid (i.e. its gravitational power) three situations can arise: i/ subduction initiates and stalls (Extended Data Fig. 3b), ii/ the slab detaches then the lid stabilizes (Figs. 1a$_{3\text{-}4}$ and Extended Data Fig. 3c), or iii/ recurrent detachment of the slab occurs until complete recycling of the oceanic lid followed by stabilisation (Extended Data Fig. 3d). When the slab reaches a depth of ~ 200 km, slab pull contributes to drive subduction and rapid rollback of the subducting lid, which in turn promotes lithospheric boudinage and continental rifting (Fig. 1a$_2$ and Extended Data Fig. 3c$_{1\text{-}3}$). Through spreading and thinning of the continent, its base rises from 225 km to ~75 km deep on average, and shallower between lithospheric boudins (Figs. 1a$_3$ and 2b and Extended Data Figs. 3c$_{2\text{-}3}$ and 3d$_{1\text{-}5}$). This triggers an episode of deep (~150 km) to shallow (<100 km) decompression melting and progressive depletion of the ambient fertile mantle (Figs. 2 and 3b). Harzburgites of the continental mantle are too refractory to melt upon decompression. Polybaric melting of fertile mantle produces a 6 km thick basalt cover and a mantle residue ~ 75 km thick with an averaged depletion of 7.5% (Figs. 2 and 3c). The bulk of depletion occurs over a volcanic episode lasting up to ~13 Myr, although partial melting persists over a duration of 45 Myr (Fig. 2b). In the last ~25 Myr of melting, the sub-continental mantle cools until melting stops (Figs. 1a$_4$ and 2). Decompression melting allows the

spreading continent to maintain a minimum chemical thickness of at least 140-150 km. Following the melting phase, conductive cooling results in the thermal thickening and strengthening of a chemically stratified cratonic lithosphere (Figs. 1a$_4$, 2 and 3d). Over the whole process, the buoyancy of the continent decreases, subduction stops and a stagnant lid regime is re-established (Fig. 1a$_4$).

Trade-offs between yield stress, gravitational stress and continental volume determine the initiation of subduction in our models (Extended Data Figs. 3b and 3d). For a yield stress of 150 to 300 MPa, consistent with recent estimates of rheological parameters of the lithospheric mantle[21,22], increasing the continent width favours subduction initiation (Extended Data Fig. 4). These results suggest an increasing potential for subduction as continental area increased through time.

Our models not only confirm important results from previous studies, but they also provide innovative explanations for key attributes of Archaean cratons. Both transient subduction and dripping styles are consistent with previous models of Archaean[23] and modern[13] subduction. As observed in previous work, the length of the detached segments increases with the yield stress of the lid[23]. Our models confirm that a combination of the buoyancy, the large viscosity of Archaean sub-continental lithospheric mantle (SCLM), and large plastic strain weakening prevent the recycling of the SCLM, which explains its longevity[24]. Our models account for the average thickness (~6 km) and duration of volcanism (~10 to 50 Myr) of greenstones covers, and predict polybaric (5 to 2 GPa) partial melting, involving deep (garnet-bearing) to shallow sources (Fig. 2). The MgO content of basaltic melts produced at these pressures ranges between 11 and 17% (Fig. 2a), consistent with komatiitic basalts (12-18% MgO) typical of Archaean greenstones[17,26]. Tholeiitic basalts (6-12% MgO), abundant in Archean greenstones[26], can be produced in our model in regions of continental necking where partial melting can occur at pressure < 3 GPa. Figure 2a shows that to account for the formation of komatiites (MgO>18%) our model would simply require a mantle potential temperature greater than 1820 K. When subduction starts, arc volcanism is expected at convergent margins while continental extension and rifting still operate (Fig. 1a$_2$). Therefore, our model can explain the metasomatism and production of sanukitoid melts through migration of younger TTG melts generated by partial melting of subducting eclogitised basaltic crust (Fig. 3c).

On modern Earth, mantle plumes mostly occur away from subduction zones[25]. Hence, the eruption

duration and sequential inter-layering of komatiite, tholeiite, calc-alkaline and felsic volcanics, ubiquitous in Archaean greenstone belts[26-28], frequently attributed to repeated interaction between mantle plumes and subduction zones over hundreds of millions of years[6], remains enigmatic. Our model predicts the co-occurrence of deep (up to 150 km) to shallow (<100 km) mafic volcanics (Fig. 2b) and arc magmatism in a self-consistent geodynamic framework.

Moreover, our model predicts a progressive chemical stratification of the SCLM concomitant with that of the continental crust and growth of the greenstone cover. This explains the strong geochemical layering of cratonic mantle inferred by geochemical and petrological studies of mantle xenolith[5]. Pure shear stretching and thinning during the collapse promotes development of a sub-horizontal litho-tectonic fabric in the refractory harzburgite and dunite, and to a lesser extent in the accreted moderately depleted mantle (Fig. 2b). The predicted litho-tectonic layering explains the seismic mid-lithospheric discontinuity around 100 km depth observed within cratons[29]. This discontinuity[7] could correspond to the sharp transition predicted by our model between the strongly stretched, strongly depleted primary root of the continent and the moderately stretched, moderately depleted-to-fertile mantle accreted through cooling (Fig. 3).

We propose that the collapse of early continents was a key process in Archaean geodynamics, resulting in the concomitant structuration of the mantle root and crust of cratons. This process would have kick-started transient episodes of plate tectonics, until plate tectonics became self-sustained, through increasing continental area[30] and decreasing buoyancy of oceanic plates[3].

METHODS SUMMARY

We solve the problem of conservation of mass, momentum and energy for incompressible mantle flow and lithosphere deformation in the top 700 km of the Earth, using the particle-in-cell finite-element code Ellipsis[12] (freely available at http://www.geodynamics.org/cig/software/ellipsis3d/). These equations are solved along with constitutive relations for visco-plastic rheology depending on temperature, stress and strain rate, and melt fraction and depletion (see Methods and Extended Data Table 1). Over 200 calculations were conducted varying the lateral extent of the model domain (4200 to 16800 km), the half-width (400 to 1400 km) and thickness (175 or 225 km) of the continents, the

limiting yield stress of mantle rocks (100 to 500 MPa), density of the top 75 km of the oceanic lid mantle (3395 down to 3360 kg m^{-3}), and various modes of melt extraction. The reference densities of all mantle rocks depend on temperature (Extended Data Table 1), and the density of basalts also depends on pressure to simulate eclogitisation. Our experiments take into account the thermo-mechanical impacts of partial melting, which allows us to map the evolution of the depletion and reveal the development of the lithospheric mantle layering. The specific version of Ellipsis and input scripts used for this work are available from the first author upon request.

[1] Bott, M. H. P. Modelling the plate-driving mechanism. *Journal of the Geological Society of London* **150**, 941-951 (1993).

[2] Faccenna, C., Giardini, D., Davy, P. & Argentieri, A. Initiation of subduction at Atlantic-type margins: Insights from laboratory experiments, *Journal of Geophysical Research* **104**, 2749-2766 (1999).

[3] Sleep, N. H. & Windley, B. F. Archean plate tectonics: constraints and inferences. *Journal of Geology* **90**, 363-379 (1982).

[4] van Hunen, J. & Moyen, J. F. Archean Subduction: Fact or Fiction? *Annual Reviews of Earth and Planetary Sciences* **40**, 195-219 (2012).

[5] Griffin, W. L., O'Reilly, S. Y., Afonso, J.-C. & Begg, G. C. The composition and evolution of lithospheric mantle: a Re-evaluation and its tectonic. *Journal of Petrology* **50**, 1185-1204 (2009).

[6] Wyman, D. A., Kerrich, R. & Polat, A. Assembly of Archean cratonic mantle lithosphere and crust: plume–arc interaction in the Abitibi-Wawa subduction accretion complex. *Precambrian Research* **115**, 37–62 (2002).

[7] Yuan, H. & Romanowicz, B. Lithospheric layering in the North American craton. *Nature* **466**, 1063-1068 (2010).

[8] Martin, H., Smithies, R. H., Rapp, R., Moyen, J. F. & Champion, D. An overview of adakite, tonalite–trondhjemite–granodiorite (TTG), and sanukitoid: relationships and some implications for crustal evolution. *Lithos* **79**, 1-24 (2005).

[9] Polat, A., Hofmann, A. W. & Rosing, M. T. Boninite-like volcanic rocks in the 3.7–3.8 Ga Isua

169 greenstone belt, West Greenland: geochemical evidence for intra-oceanic subduction zone processes
170 in the early Earth. *Chemical Geology* **184**, 231-254 (2002).
171 [10] Harrison, T. M. et al. Heterogeneous Hadean hafnium: Evidence of continental crust at 4.4 to 4.5
172 Ga. *Science* **310**, 1947-1950 (2005).
173 [11] van Thienen, P., Vlaar, N.J., van den Berg, A.J., Assessment of the cooling capacity of plate
174 tectonics and flood volcanism in the evolution of Earth, Mars and Venus. *Physics of the Earth and*
175 *Planetary Interiors* **150**, 287-315 (2005).
176 [12] Moresi, L., Dufour, F. & Muhlhaus, H.-B. A Lagrangian integration point finite element method
177 for large deformation modeling of viscoelastic geomaterials. *J. Comput. Phys.* **184**, 476–497 (2003).
178 [13] Nikolaeva, K., Gerya, T. V., & Marques, F. O. Subduction initiation at passive margins:
179 numerical modeling. *Journal of Geophysical Research* **115**, doi:10.1029/2009JB006549 (2010).
180 [14] Bailey, R. Gravity-driven continental overflow and Archaean tectonics. *Nature* **398**, 413-415
181 (1999).
182 [15] Rey, P. F. & Coltice, N. Neoarchean lithospheric strengthening and the coupling of the Earth's
183 geochemical reservoirs. *Geology* **36**, 635–638 (2008).
184 [16] Bédard, J. H. A catalytic delamination-driven model for coupled genesis of Archaean crust and
185 sub-continental lithospheric mantle. *Geochimica Cosmochimica Acta* **70**, 1188-1214 (2006).
186 [17] Arndt, N. T., Coltice, N., Helmstaedt, H. & Michel, G. Origin of Archean subcontinental
187 lithospheric mantle: Some petrological constraints. *Lithos* **109**, 61-71 (2009).
188 [18] Zhang, C. et al. Constraints from experimental melting of amphibolite on the depth of formation
189 of garnet-rich restites, and implications for models of Early Archean crustal growth. *Precambrian*
190 *Research* **231**, 206-217 (2013).
191 [19] Huppert, H. E. Propagation of two-dimensional and axisymmetric viscous gravity currents over
192 a rigid horizontal surface. *Journal of Fluid Mechanics* **121**, 43-58 (1982).
193 [20] Moresi, L. & Solomatov, V. Mantle convection with a brittle lithosphere: thoughts on the global
194 tectonic styles of the Earth and Venus. *Geophysical Journal International* **133**, 669-682 (1998).
195 [21] Demouchy, S., Tommasi, A., Ballaran, T. B. & Cordier, P. Low strength of Earth's uppermost
196 mantle inferred from tri-axial deformation experiments on dry olivine crystals. *Physics of the Earth*

197 *and Planetary Interiors* **220**, 37-49 (2013).
198 [22] Zhong, S. & Watts, A. B. Lithospheric deformation induced by loading of the Hawaiian Islands
199 and its implications for mantle rheology. *Journal of Geophysical Research* **118**,1-24 (2013).
200 [23] van Hunen, J. & van den Berg, A. P. Plate tectonics on the early Earth: limitations imposed by
201 strength and buoyancy of subducted lithosphere. *Lithos* **103**, 217-235 (2008).
202 [24] Lenardic, A., Moresi, L.-N & Mühlaus H. Longevity and stability of cratonic lithosphere:
203 Insights from numerical simulations of coupled mantle convection and continental tectonics. *Journal*
204 *of Geophysical Research* **108**, doi:10.1029/2002JB001859 (2003).
205 [25] Cazenave, A., Souriau, A. & Dominh, K. Global coupling of Earth surface topography with
206 hotspots, geoid and mantle heterogeneities. *Nature* **340**, 54-57 (1989).
207 [26] Sproule, R. A., Lesher, C. M., Ayer, J., Thurston, P. C. & Herzberg, C. T. Spatial and temporal
208 variations in the geochemistry of komatiitic rocks in the Abitibi greenstone belt. *Precambrian*
209 *Research* **115**, 153-186 (2002).
210 [27] Ayer, J. et al. Evolution of the southern Abitibi greenstone belt based on U–Pb geochronology:
211 autochthonous volcanic construction followed by plutonism, regional deformation and sedimentation.
212 *Precambrian Research* **115**, 63-95 (2002).
213 [28] Bateman, R., Costa, S., Swe, T. & Lambert, D. Archaean mafic magmatism in the Kalgoorlie
214 area of the Yilgarn Craton, Western Australia: a geochemical and Nd isotopic study of the
215 petrogenetic and tectonic evolution of a greenstone belt. *Precambrian Research* **108**, 75-112 (2001).
216 [29] Kind, R., Yuan, X. & Kumar, P. Seismic receiver functions and the lithosphere–asthenosphere
217 boundary. *Tectonophysics* **536-537**, 25-43 (2012).
218 [30] Rolf, T. & Tackley, P. J. Focussing of stress by continents in 3D spherical mantle convection
219 with self-consistent plate tectonics. *Geophysical Research Letters* **38**, doi:10.1029/2011GL048677
220 (2011).
221
222 **Acknowledgements** P.F.R acknowledges the assistance of resources provided at the NCI National
223 Facility systems at the Australian National University through the National Computational Merit
224 Allocation Scheme supported by the Australian Government. N.C was supported by the Institut

225 Universitaire de France, and the European Research Council within the framework of the SP2-Ideas
226 Program ERC-2013-CoG, under ERC Grant agreement number 617588. NF was supported by Statoil
227 ASA.

228 **Author contributions** Conceptual idea P.F.R, numerical experiments P.F.R. and N.C., interpretation
229 of the results P.F.R, N.C. and N.F., writing of the manuscript P.F.R., N.C. and N.F.

230 **Author information** Reprints and permissions information is available at www.nature.com/reprints.
231 The authors declare no competing interests. Readers are welcome to comment on the online version of
232 the paper. Correspondence and requests for Ellipsis code and input scripts should be addressed to
233 P.F.R. (patrice.rey@sydney.edu.au).

234

235 **Figure 1 | Numerical solution of an example of continent collapse leading to subduction.**
236 Modelling setup (**a_0**) and computed snapshots (**a_{1-4}**) for a 700-km-deep, 6300-km-long box including a
237 225-km-thick continent, of half-width 800 km. All mantle rocks have a limiting yield stress of
238 300 MPa. Mantle cooler than 1620 K is in blue (darker blue is hotter), mantle hotter than 1620 K is in
239 pink (darker pink is hotter). Regions of depletion due to partial melting of ambient fertile mantle are
240 hatched. Compositional structure, reference densities and reference rheological profile are shown in
241 (**b_1**) for the continent, and (**b_2**) for the adjacent lithospheric lid. This numerical solution documents the
242 long phase of slow continental spreading leading to the initiation of a slab (**a_{1-2}**). Once the slab
243 reaches a depth of ~200 km, slab pull contributes to drive subduction, rollback and continental
244 boudinage (**a_2**, in some experiments boudinage leads to rifting) and slab detachment (**a_3**). In this
245 experiment, the detachment of the slab is followed by a long period of thermal relaxation and
246 stabilisation during which the thickness of the continent increases through cooling and incorporation
247 of the moderately depleted mantle (**a_4**).

248 **Figure 2 | Layering of the continental lithosphere through thinning and progressive accretion of**
249 **moderately depleted mantle.** a/ Points located at depth A_0 to A_3 before spreading, are exhumed
250 during spreading to locations A_0' to A_3' following the blue pressure-temperature-time (P-T-t) path.
251 The geotherm intersects the solidus and the temperature in the partially molten column remains close
252 to the solidus because latent heat is continuously extracted with the melt once melt fraction reaches

1%. Melt is extracted from various depths following the melt adiabat (yellow arrows). The region between the hydrous fertile mantle solidus and liquidus is mapped for MgO content (see Method). The deeper part of the column produces komatiitic basalts (dark blue shading), while partial melting at pressure < 3 GPa produces tholeiitic basalts (pale blue shading). b/ Temporal evolution of the laterally averaged depletion (cyan), partial melting (yellow), and density interfaces (thick dashed lines). As spreading and thinning proceeds, pure shear fabrics (shown as finite strain ellipses) develop in the refractory mantle and in the moderately depleted mantle, which records a shorter strain history. The base of the partially molten column remains close ~150 km whereas its top progressively rises from ~150 km at the beginning of partial melting (at ~44 Myr) to an average of ~75 km below the surface (at ~55 Myr). From 55 Myr, spreading slows down and progressive cooling reduces the amount of melt, until partial melting stops at ~82 Myr. This results in the progressive chemical stratification of the sub-continental lithospheric mantle.

Figure 3 | Proposed model for the co-evolution of cratonic crust and sub-continental lithospheric mantle. Integrating the results of our numerical experiments with petrological data supports a model linking the formation of continents to the initiation of subduction at their margins, through the process of continent collapse. This model predicts the layering of the sub-continental lithospheric mantle (SCLM), polybaric and multimodal volcanism recorded in greenstone covers, and the metasomatism of the SCLM. **a**, Deep mantle partial melting leads to the formation of an oceanic plateau that differentiates into a continent. The residue of mantle melting forms the strongly depleted harzburgite root of the continent, while the deeper part of the basaltic crust differentiates via partial melting into tonalite-trondjhemite-granodiorite (TTG). **b**, As the continent grows in thickness and length, excess gravitational potential energy drives its collapse and the shortening of the adjacent oceanic lid (in grey). During collapse and thinning of the continent, decompression melting (yellow) of the fertile ambient mantle and extraction of deep (komatiitic basalt) to shallow (tholeiite) melt contribute to the growth of the greenstone cover, and to the formation of a moderately depleted mantle layer. **c**, Due to the horizontal push of the collapsing continent, the thickened margin of the oceanic lid subducts underneath the continental margin. Partial melting of the thick, eclogitised oceanic crust produces TTG melts (purple), which metasomatise both the mantle wedge and the

lithospheric mantle. Melting of the hydrated and metasomatised mantle wedge produces calc-alkaline to sanukitoid melts (orange). **d**, Following the detachment of the slab, and once the gravitational power of the continent is too small deform its surrounding, the continent thicken through thermal relaxation and cooling, first incorporating the layer of moderately depleted mantle and then a layer of un-melted fertile mantle.

METHODS

We use Ellipsis, a Lagrangian integration point finite-element code[12,31], to solve the governing equations of momentum, mass and energy in incompressible flow. Our reference Cartesian 2D numerical model is 700 km deep and 6300 km long. The Stokes equation that balances buoyancy forces, viscous stresses and pressure gradients is solved on a Eulerian computational grid made of 32 x 288 cells with uniform spacing. We have verified validity of our results by testing a higher resolution grid of 64 x 576 cells. Each cell is populated by 100 Lagrangian particles (total > 920,000 particles) tracking the material properties and therefore material interfaces during mantle flow and lithospheric deformation. A free slip condition is applied to the vertical and horizontal boundaries of the modelling domain. The temperature in the upper horizontal boundary is maintained at 293 K, while the base is maintained at 1873 K.

Each material is characterised by a range of thermal and mechanical properties (Extended Data Table 1) including: density, coefficient of thermal expansion, heat capacity (1000 J kg^{-1} K^{-1}), heat diffusivity (9×10^{-7} m^2 s^{-1}), radiogenic heat production, cohesion, coefficient of friction, limiting pressure-independent yield stress, dislocation creep parameters (*A, n, E*, Extended Data Table 1), and limiting lower and upper viscosities respectively 10^{18} Pa s and 5×10^{23} Pa s.

Our strategy consists in setting up a model in which the mantle convects under a stagnant lid, the top 15 km of which are made of weak basaltic crust simulating hydrothermally altered basalts (Extended Data Fig. 2). After reaching steady-state equilibrium, the temperature field is laterally averaged (Extended Data Fig. 2) and linearised (i.e. temperature at the surface is 293 K, temperature at 150 km depth and below is 1820 K). This ensures that no convective stress acts on the lid in the initial condition. Finally, we replace a segment of the oceanic lid by a continent made of depleted mantle

underneath a continental crust. We take advantage of the symmetry of the model, and we insert the continent along the left side of the model.

We model the mantle as a visco-plastic material with temperature, stress, strain-rate and melt dependent viscosity. The viscous rheology of the mantle is based on dry olivine[32] (Extended Data Table 1). Its plastic rheology is approximated with a Coulomb failure criterion[33] with cohesion 40 MPa, a coefficient of friction (μ_{ref}) 0.268, and a weakening factor dependent on the accumulated plastic strain (ε_p). The coefficient of friction (μ) evolves as a function of the total plastic strain as:

for $\varepsilon_p < 0.15$: $\mu = \mu_{ref} \times (1-(1-0.0373) \times (\varepsilon_p / 0.15)^{0.25})$

for $\varepsilon_p > 0.15$: $\mu = \mu_{ref} \times 0.0373$

This weakening leads to fault-like strain localisation with nominal viscosity ~25 times weaker than that of the surrounding rocks when plastic strain reaches 15%. This weakening, which is a key factor for the operation of plate tectonics on present Earth[20], simulates the formation of phyllosilicates (serpentine, talc, micas) during the strain-induced hydration of mantle rocks and basalts. For semi-brittle deformation independent of pressure, we impose an upper limiting yield stress[34,35] in the range of 100 to 500 MPa.

The top 15 km of the model consist of a thick layer of basalts, which simulates both the oceanic crust, and the greenstone cover on the Archaean continent. Because these basalts were largely emplaced below sea level[36], they are strongly hydrothermally altered. For simplicity, we assume that this layer has a nominal viscosity 1000 times weaker that the underlying mantle, a weak cohesion of 1 MPa, a reference coefficient of friction of 0.134 and the same weakening properties than the rest of the lid. This weak layer of basalt helps the decoupling between the subducting slab and the upper plate allowing for one side subduction. It also mitigates the absence of free surface, by allowing the upper plate to bend downward more realistically to form a deeper trench. The reference density of this material (3000 kg m^{-3}) is sensitive to pressure, and increases upon burial up to 3540 kg m^{-3} to simulate eclogitisation[37]. When subduction initiate, this weak material lubricates the Benioff plane, which, with eclogitisation, facilitates subduction by decoupling the slab from the continental margin. This simulates the impact of slab dehydration, which in nature lubricates the Benioff plane.

Modelling continent differentiation is beyond the scope of this paper, and we simply replace a 400 to 1200 km long segment of the oceanic lid by a continent, which includes a 40-km-thick crust (density 2850 kg m^{-3}), covered by a 15 km thick flood basalt (density 3000 kg m^{-3}). This crust stands above 170 km of depleted mantle (density 3310 kg m^{-3}) with a nominal viscosity 100 times stronger than the adjacent lid to account for dehydration[38]. We assume the same limiting yield stress than that of other mantle rocks that we vary in the range of 100 to 500 MPa. The continental crust is assumed to be 100 times more viscous than a weak mafic granulite[39] (Extended Data Table 1). A limiting yield stress of 250 MPa is imposed in the crust to simulate semi-brittle regime. This strong continent represents a significant buoyant anomaly, imparting a horizontal gravitational force on its surrounding.

We use the hydrous mantle solidus and liquidus of ref. 40 to model partial melting in the sub-continental fertile mantle. For the depleted root of the continent we increase the hydrous mantle solidus by 200 K, a reasonable assumption for the harzburgite solidus[41]. Melt fraction is calculated at each time step using eq. 21 of ref. 42, whereas MgO content of accumulated melt in Fig.2 is calculated using ref. 43. Because decompression and exhumation of the mantle occur very slowly (~ 1 to 4 mm y^{-1}) at the pace imposed by the spreading of the continent, one can expect the melt to segregate and to pond at the top of the partially molten column, before it escapes to the surface through dikes. Therefore, we assume that melt in the partially molten column is extracted when the melt fraction reaches 1%. In this case, latent heat escapes with the melt, and the ascending depleted residue follows the solidus closely. We assume the fusion entropy to be 400 J kg^{-1} K^{-1}. We have also tested the isentropic case in which the melt stays in the source. In this case, lithospheric boudinage controls continental spreading rather than homogeneous thinning.

The small fraction of melt (<1%) has only a modest impact on the buoyancy of the partially molten region. However, the density of the residue decreases as it becomes more depleted. We assume a maximum density decrease of 1.5% upon full depletion. Because even a small fraction of melt lubricates grain boundaries, it affects the viscosity of the partially molten column. Hence, we impose a linear viscosity drop to a maximum of one order of magnitude when the melt fraction reaches 1%. On the other hand, partial melting drains water out of the solid matrix and reduces the number of

363 phases. Although the impact of dehydration on the viscosity may not be as significant as previously
364 thought[44], both processes should contribute to increase the viscosity of the depleted residue once its
365 temperature drops below the solidus. In our experiment we impose an increase in viscosity
366 proportional to depletion, assuming a viscosity increase of two orders of magnitude for 100%
367 depletion.
368
369
370 [31] O'Neill C., Moresi, L., Müller, R. D., Albert, R. & Dufour, F. Ellipsis 3D: A particle-in-cell
371 finite-element hybrid code for modelling mantle convection and lithospheric deformation. *Computer*
372 *& Geosciences* **32**, 1769-1779 (2006).
373 [32] Brace, W. F., Kohlstedt, D. L. Limits on lithospheric stress imposed by laboratory experiments.
374 *Journal of Geophysical Research* **85**, 6248-6252 (1980).
375 [33] Byerlee, J. D. Brittle–ductile transition in rocks. *Journal of Geophysical Research* **73**, 4741–4750
376 (1968).
377 [34] Ord, A., Hobbs, B. E. The strength of the continental crust, detachment zones and the
378 development of plastic instabilities. *Tectonophysics* **158**, 269- 289 (1989).
379 [35] Escartin, J. & Hirth, G. Nondilatant brittle deformation of serpentinites: Implications for Mohr-
380 Coulomb theory and the strength of faults. *Journal of Geophysical Research* **102**, 2897-2913 (1997).
381 [36] Flament, N., Coltice, N. & Rey, P. F.. A case for late-Archaean continental emergence from
382 thermal evolution models and hypsometry. *Earth and Planetary Science Letters* **275***,* 326-336 (2008).
383 [37] Aoki, I. & Takahashi, E. Density of MORB eclogite in the upper mantle. *Physics of the Earth*
384 *and Planetary Interiors* **143-144**, 129-143 (2004).
385 [38] Hirth. G. & Kohlstedt, D. Rheology of the upper mantle and the mantle wedge: A view from the
386 experimentalists, in *Inside the subduction factory,* John Eiler (editor), *Geophysical Monograph* **138**,
387 83-105, American Geophysical Union doi:10.1029/138GM06 (2003).
388 [39] Wang, Y. F., Zhang, J. F., Jin, Z. M. & Green, H. W. Mafic granulite rheology: Implications for a
389 weak continental lower crust. *Earth Planetary and Science Letters* **353-354**, 99-107 (2012).
390 [40] Katz, R. F., Spiegelman, M. & Langmuir, C. H. A new parameterization of hydrous mantle

391 melting. *Geochemistry, Geophysics Geosystems* **4** , doi:10.1029/2002GC000433 (2003).
392 [41] Maaløe, S. The solidus of harzburgite to 3 GPa pressure: the compositions of primary abyssal
393 tholeiite. *Mineralogy and Petrology* **81**, 1-17 (2004).
394 [42] McKenzie, D. & Bickle, M. J. The volume and composition of melt generated by extension on
395 the lithosphere. *Journal of Petrology* **29**, 625-629 (1988).
396 [43] Herzberg, C. & Gazel, E. Petrological evidence for secular cooling in mantle plumes. *Nature* **458**,
397 619-623 (2009).
398 [44] Fei, H., Wiedenbeck, M., Yamazaki, D. & Katsura, T. Small effect of water on upper-mantle
399 rheology based on silicon self-diffusion coefficients. *Nature* **498**, 213-216 (2013).
400

401 **Extended Data Figure 1| Gravitational force between continent and oceanic lid. a**, Depth profile
402 of the difference in lithostatic pressure σ_{zz} between an oceanic lid 150 km thick and a continent (1)
403 150 km, (2) 200 km and (3) 250 km thick. The vertical integration of the lithostatic pressure
404 difference ($\Delta\sigma_{zz}$) is the resulting gravitational force *Fg* acting between the Archaean continent and the
405 adjacent lithospheric lid. In all cases, this force is $> 7\times10^{13}$ N m^{-1}, comparable to or larger than the
406 present-day tectonic forces driving orogenesis[1]. **b**, Reference density structure of the continent and
407 oceanic lithosphere (densities of depleted and fertile mantle are from Ref. 5). All densities vary with
408 temperature with a coefficient of thermal expansion $\alpha = 3\times10^{-5}$ K^{-1}. We assume a linear geotherm in
409 the oceanic plate ($T_{(z=0)}$= 293 K, $T_{(z=150km)}$= 1820 K) above a convective mantle with an average
410 temperature of 1820 K.
411 **Extended Data Figure 2 | Stagnant lid convection model before lateral averaging and**
412 **introduction of a continent.** The temperature field in our experiments derives from the lateral
413 averaging of an experiment in which the mantle is let to convect under constant top boundary
414 temperatures (293 K) and internal radiogenic heat production (1.36×10^{-8} W m^{-3}). The coefficient of
415 thermal expansion is equal to 3×10^{-5} K^{-1}, the thermal diffusivity to 0.9×10^{-6} m^2 s^{-1} and the heat
416 capacity to 1000 J kg^{-1} K^{-1}, and the Rayleigh number of the convecting mantle is between 10^6 and 10^7.
417 The snapshot shows the temperature field after ~1 Gyr of evolution. In this experiment, a lid develops
418 that remains stagnant. The formation of cold drips from the lower, unstable, part of the stagnant lid,

and conductive cooling balance each other to maintain the thickness of the stagnant lid. In the lid, the conductive geotherm is such that a temperature of 1620 K is reached at ~100 km depth, and 1820 K (the average temperature in the convecting mantle) is reached at ~150 km depth.

Extended Data Figure 3 | Numerical solutions for various models showing contrasting tectonic evolution. a, In this experiment, all parameters are as in Fig. 1 except the continent half-width that is 500 km. In the case of stable continental collapse, cold drips form faster than subduction can initiate, which stabilises the oceanic lid. $\mathbf{a_1}$, During and after spreading and thinning of the continent, a layer of mostly fertile mantle is accreted at the base of the continent through cooling. **b**, This experiment is in all aspects similar to that presented in Fig. 1, but for the oceanic lid that includes 75 km of buoyant lithopheric mantle (in purple) with a reference density of 3365 kg m^{-3} (i.e. 35 kg m^{-3} less dense than non-depleted mantle rocks). $\mathbf{b_{0\text{-}1}}$, shows i/ homogeneous continental spreading with decompression melting, and ii/ the initiation of a slab which stalls underneath a long-lived orogenic wedge. The same experiment with a buoyant mantle lid with a reference density of 3370 kg m^{-3} leads to subduction. $\mathbf{b_{2\text{-}3}}$, However, because of its buoyancy the oceanic slab stalls, although the very base of the oceanic lid is dragged into the asthenosphere. **c**, In this experiment, the continent has a half-width of 600 km and all mantle rocks have a limiting yield stress of 200 MPa. **d**, In this experiment, the limiting yield stress of the strongly depleted continental mantle (in green) is increased to 500 MPa to take into account the possible plastic strengthening of the depleted, and therefore dry, mantle (all other mantle rocks have a limiting yield stress of 300 MPa). Comparison to Fig. 1 - which shows the same experiment but with all mantle rocks with a limiting yield stress of 300 MPa - illustrates that a stronger continent deforms in a more heterogeneous manner since following an episode of spreading and thinning ($\mathbf{d_1}$), strain localisation and rifting divide the continent in two ($\mathbf{d_2}$), before stabilisation and cooling ($\mathbf{d_3}$). $\mathbf{d_{0\text{-}2}}$, The continental spreading is heterogeneous, subduction of the oceanic lid initiates, the slab detaches and a continental rift initiates. $\mathbf{d_3}$, Continental rifting, recurrent slab detachment and trench-retreat occur, and two continental blocks move away from each other with little internal deformation. $\mathbf{d_{4\text{-}5}}$, Rifting and subduction stop, while cooling re-establish a stagnant lid. In all cases, a protracted phase of decompression melting lasting several tens of Myr is coeval with spreading and rifting.

Extended Data Figure 4 | Tectonic phase diagram: subduction versus stable lid regime as a function of yield stress and continent width. Two series of calculations were carried out (with continental thickness of 175 km and 225 km), systematically varying the half-width of the continent (from 400 to 1200 km) and the limiting yield stress of all mantle rocks (from 100 to 500 MPa). Depending on the competition between the gravitational driving power of the buoyant continent and the combined viscous resistance of the continent and oceanic lid, the continental collapse either leads to the subduction of the oceanic lid under the continental margin, or not. Coloured dots and the continuous black thick line represent outcomes of numerical experiments for the 175 km thick continent. The thick dashed line separates the stable-lid domain from the subduction domain in the case of the 225 km thick continent. The arrow illustrates that continental rifting, because it reduces the half-width of continents, stabilises Archaean oceanic lids.

Extended Data Table 1 | Thermal and mechanical parameters

	Reference Density ($kg\ m^{-3}$)	Thermal expansion (K^{-1})	Radiogenic Heat ($W\ kg^{-1}$)	Cohesion (MPa)	Coefficient of friction	Limiting yield stress (MPa)	A ($MPa^{-n}\ s^{-1}$)	E ($kJ\ mol^{-1}$)	n
Continental crust	2850	0	$2.52\ 10^{-10}$	40	0.268	250	$2\ 10^{-2}$	244	3.2
Basalts	3000	0	$2.52\ 10^{-10}$	1	0.134	50	$7\ 10^{7}$	520	3
SCLM	3310	$3\ 10^{-5}$	$4\ 10^{-12}$	40	0.268	100-500	$7\ 10^{2}$	520	3
Mantle	3395	$3\ 10^{-5}$	$4\ 10^{-12}$	40	0.268	100-500	$7\ 10^{4}$	520	3

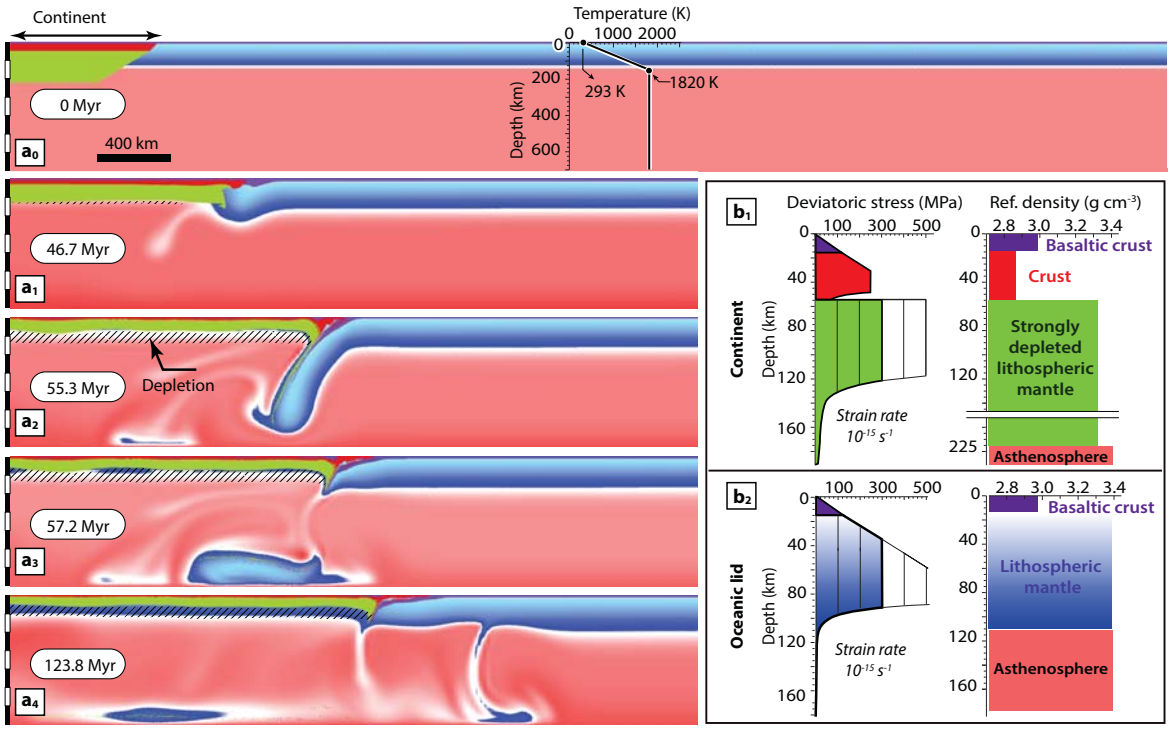

Figure 1 | Numerical solution of an example of continent collapse leading to subduction.

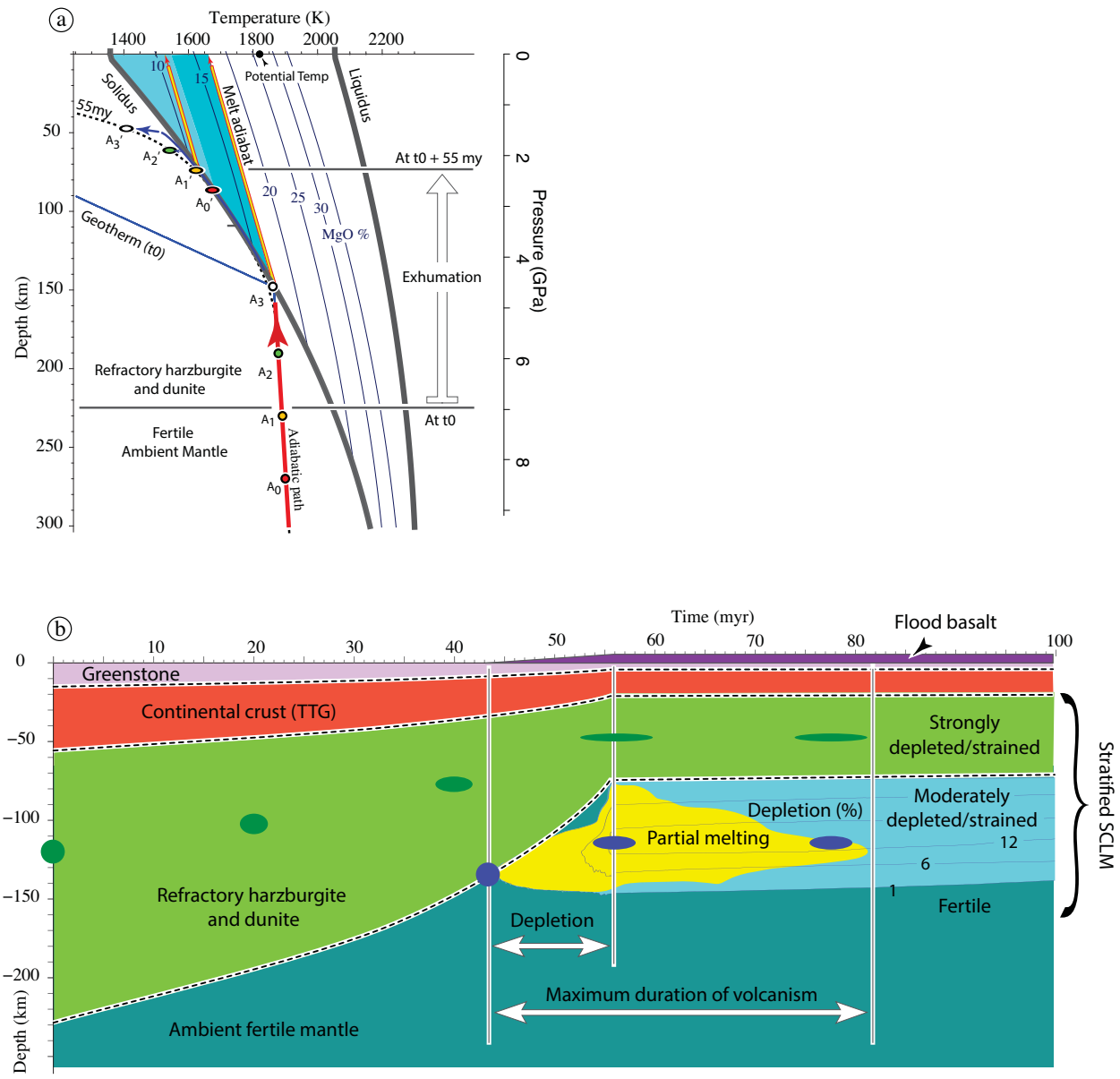

Figure 2 | Layering of the continental lithosphere through thinning and progressive accretion of moderately depleted mantle.

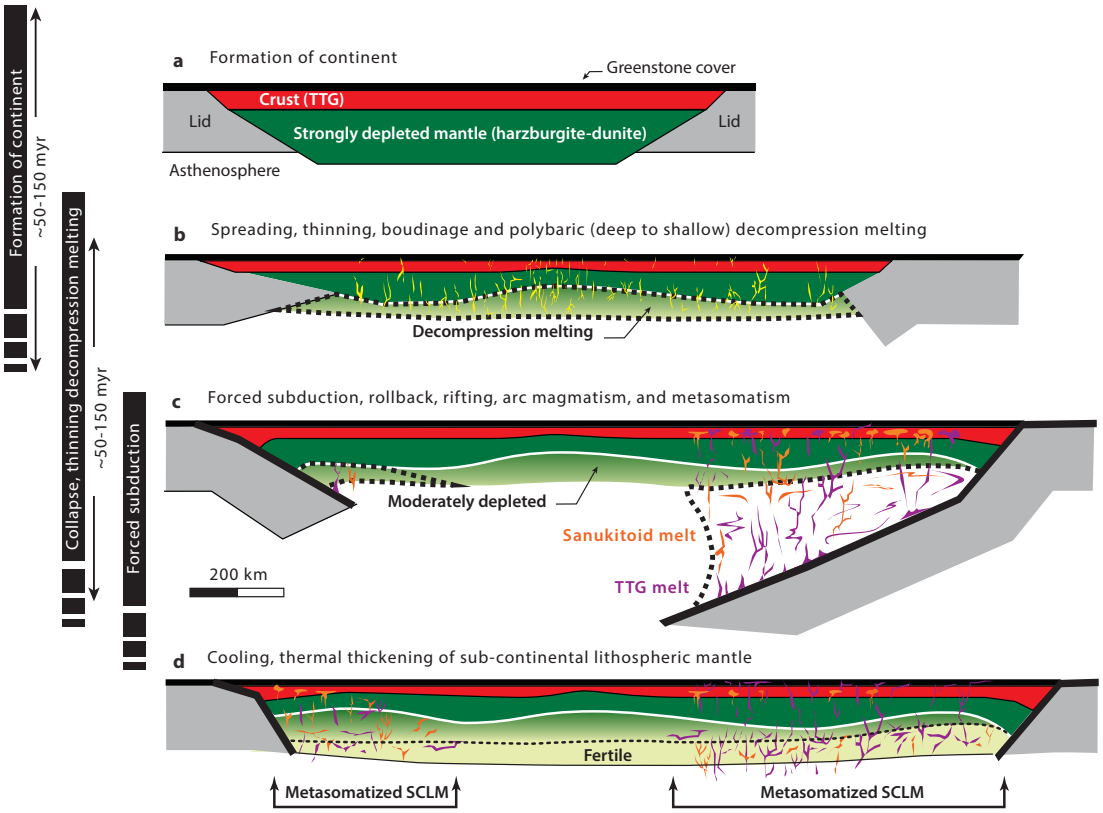

Figure 3 | Proposed model for the co-evolution of cratonic crust and subcontinental lithospheric mantle.

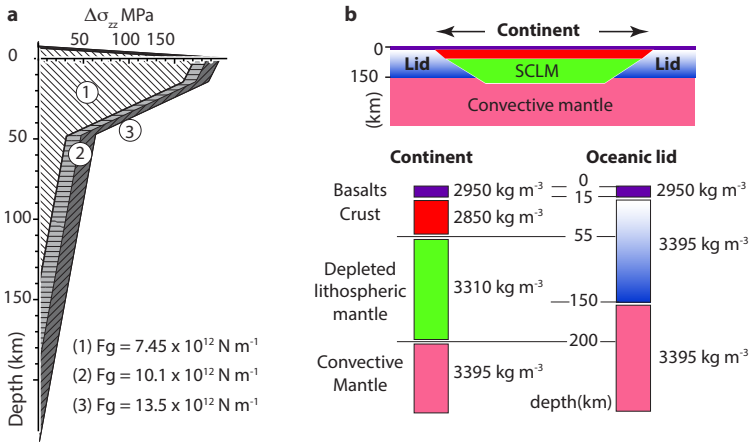

Extended Data Figure 1| Gravitational force between continent and oceanic lid.

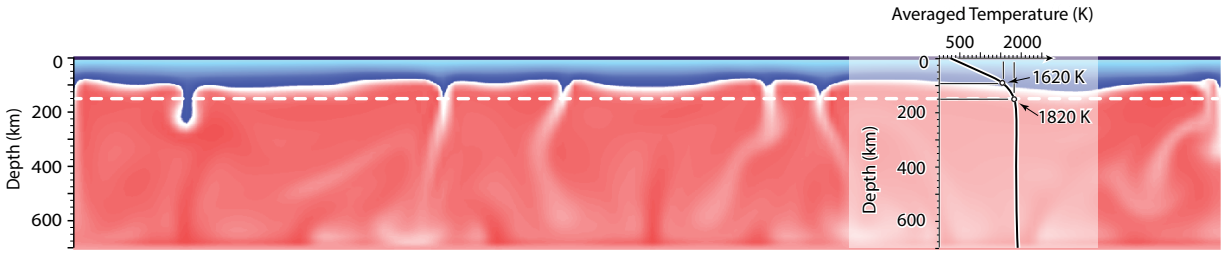

Extended Data Figure 2 | Stagnant lid convection model before lateral averaging and introduction of a continent.

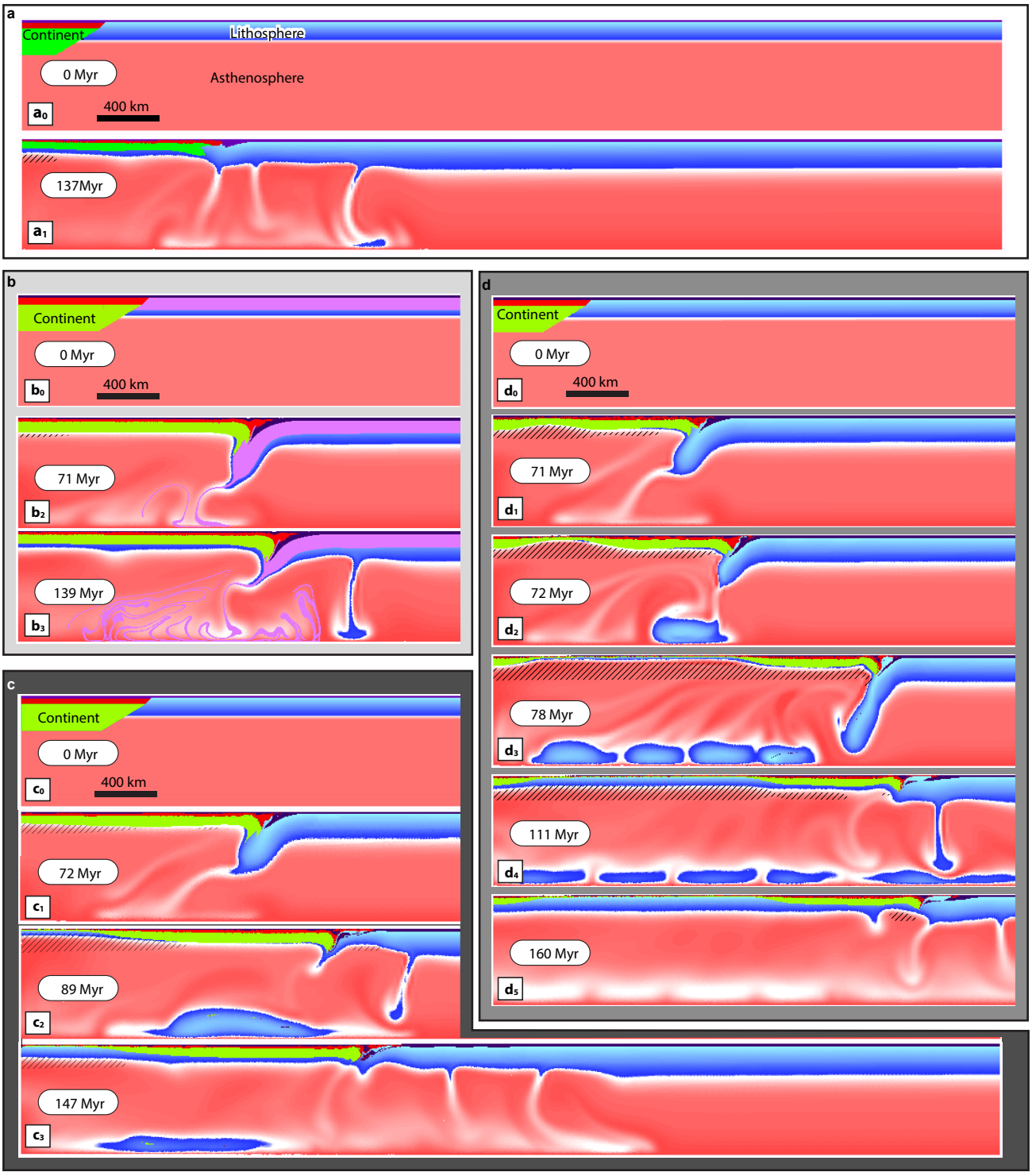

Extended Data Figure 3 | Numerical solutions for various models showing contrasting tectonic evolution.

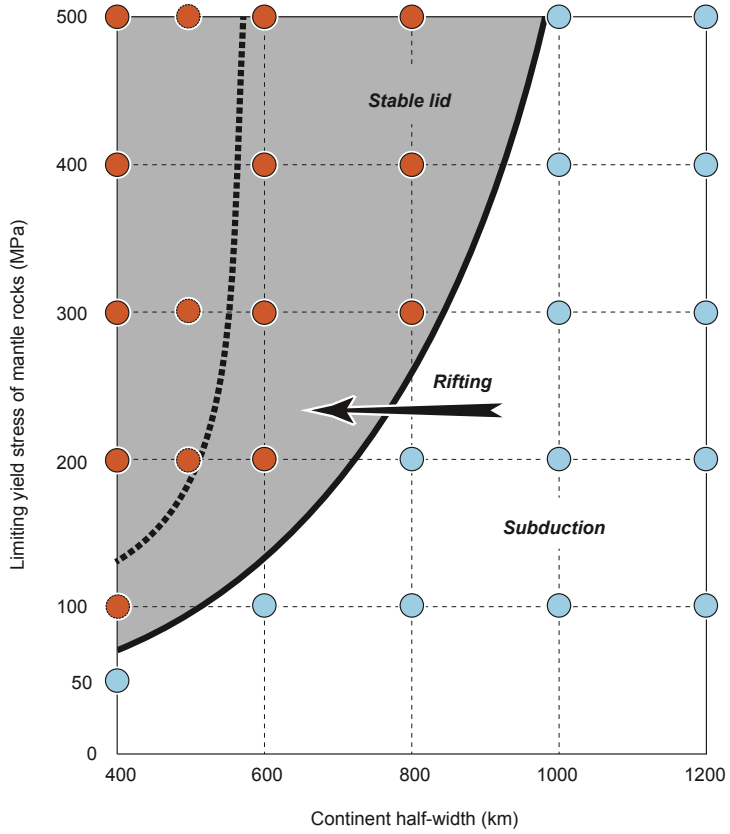

Extended Data Figure 4 | Tectonic phase diagram: subduction vs stable lid regime as a function of yield stress and continent width.